Journal of Organometallic Chemistry 694 (2009) 3518–3525

Contents lists available at ScienceDirect

Journal of Organometallic Chemistry

journal homepage: www.elsevier.com/locate/jorganchem

Syntheses, structures, spectroscopic, electrochemical properties and DFT calculation of Ru(II)–thioarylazoimidazole complexes

T.K. Mondal [a], J.-S. Wu [b], T.-H. Lu [b], Sk. Jasimuddin [c], C. Sinha [a,*]

[a] Department of Chemistry, Inorganic Chemistry Section, Jadavpur University, Kolkata 700 032, India
[b] National Tsing Hua University, Hsinchu, Taiwan 300, ROC
[c] Assam University, Silchar, Assam, India

ARTICLE INFO

Article history:
Received 16 February 2009
Received in revised form 15 June 2009
Accepted 18 June 2009
Available online 24 June 2009

Keywords:
Ruthenium(II)–azoimidazoles
X-ray structure
Electrochemistry and DFT calculation

ABSTRACT

The reaction of 1-alkyl-2-{(*o*-thioalkyl)phenylazo}imidazoles (SRaaiNR) (**2a/2b**) with Ru(II) has synthesized $[Ru(SRaaiNR)_2](ClO_4)_2$ (**3a/3b**) in 2-methoxyethanol. The reaction in methanol, however, has synthesized [Ru(SRaaiNR)(***S***RaaiNR)Cl](ClO_4) (**4a/4b**). The solid phase reaction of SRaaiNR and $RuCl_3$ on silica gel surface upon microwave irradiation has synthesized [Ru(SRaaiNR)(**S**aaiNR)](PF_6) (**5a**/**5b**) [SRaaiNR represents tridentate *N*,*N*′,*S*-chelator; ***S***RaaiNR is *N*,*N*′-bidentate chelator where ***S*** does not coordinate and **S**aaiNR refers *N*,*N*′,**S**-chelator where **S** refers to thiolato binding]. The structural characterization of [Ru(SEtaaiNEt)(***S***EtaaiNEt)Cl](ClO_4) (**4b**) and [Ru(SEtaaiNEt)(SaaiNEt)](PF_6) **(5b)** has been confirmed by single crystal X-ray diffraction study. The IR, UV–Vis, and ^{1}H NMR spectral data also support the stereochemistry of the complexes. The complexes show metal oxidation, Ru(III)/Ru(II), and ligand reductions (azo/azo$^-$, azo$^-$/azo$^{=}$). The molecular orbital diagram has been drawn by density functional theory (DFT) calculation. Normal mode of analysis has been performed to correlate calculated and experimental frequencies of representative complexes. The electronic movement and assignment of electronic spectra have been carried out by TDDFT calculation both in gas and acetonitrile phase.

1. Introduction

The coordination complexes of transition metals with azo-ligands are of current attraction due to the interesting physical, chemical, photophysical and photochemical, catalytic, biological and different material properties. The π-acidity and metal binding ability of azo nitrogen have drawn attention to the exploration of the chemistry of metal complexes incorporating azo-ligands [1–8]. Notable examples of these ligands are arylazobenzene [9], arylazooxime [10], arylazophenol [11], arylazopyridine [7,8,12], arylazoimidazole [13], arylazopyrimidine [14], arylazoaniline [15], azoantipyrene [16] and related ligands. We are engaged for last decade in the designing of azo-conjugated ligands and their metal complexes [13,14]. The synthesis of ligands in the framework of diimine (–N=C–C=N–) [17,18] and azoimine functions (–N=N–C=N–) [13] are of interest in the recent years of chemical research. Recently we have synthesized thioarylazoimidazoles (**1** and **2** in Scheme 1) [19], a tridentate *N*(imidazole), *N*(azo) and S(thioether) chelating molecule. In this work we report ruthenium(II) complexes of 1-alkyl-2-{(*o*-thioalkyl)phenylazo}imidazoles (SRaaiNR) and their reactions. We observe also ruthenium mediated selective C–S bond cleavage when reaction is carried out on silica surface under microwave irradiation. Metal mediated cleavage of carbon–sulfur bonds into carbon–hydrogen or carbon–carbon bonds under homogeneous or heterogeneous condition have diverse application in synthetic chemistry, bioinorganic chemistry and petroleum industry [20–22]. The reaction condition has influenced the efficiency, rate and nature of the products. The electronic structures of the precursor and product have been calculated by density functional theory (DFT). The spin-allowed singlet–singlet electronic transitions of the studied compounds have been calculated with the time dependent DFT method (TDDFT method), and a good agreement with the experimental spectra has been observed.

2. Results and discussion

2.1. Synthesis and formulation

Thioarylazoimidazole belongs to tridentate *N*,*N*′,*S* donor system. They are synthesized (Scheme 1) by coupling *o*-(thioalkyl)phenyldiazonium ions with imidazole in aqueous sodium carbonate and purified by solvent extraction and chromatographic process [19]. The alkylation is carried out by adding alkyliodide (MeI, EtI) in dry THF solution to the corresponding 2-{*o*-(thioalkyl)phenylazo}imidazole (**2**) in the presence of sodium hydride. They are abbreviated as SRaaiNR. The donor centres are *N*(imidazole), (N), *N*(azo) (*N*′) and thioether (S).

* Corresponding author. Fax: +91 033 2413 7121.
E-mail addresses: tkmondal_ju@yahoo.com (T.K. Mondal), c_r_sinha@yahoo.com (C. Sinha).

0022-328X/$ - see front matter © 2009 Elsevier B.V. All rights reserved.
doi:10.1016/j.jorganchem.2009.06.021

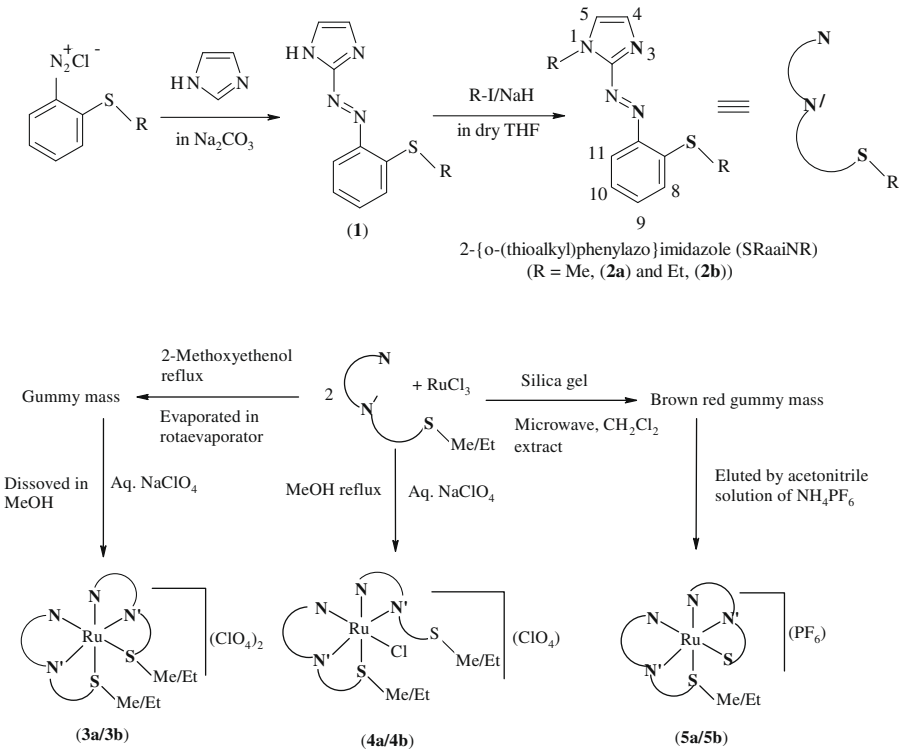

[Ru(SRaaiNR)$_2$](ClO$_4$)$_2$: R = Me (**3a**), Et (**3b**); [Ru(SRaaiNR) (**S**RaaiNR)Cl](ClO$_4$) : R = Me (**4a**), Et (**4b**); [Ru(SRaaiNR) (**S**aaiNR)](PF$_6$) : R = Me (**5a**), Et (**5b**)

Scheme 1.

[Ru(SRaaiNR)$_2$](ClO$_4$)$_2$ (**3a/3b**) are prepared by refluxing RuCl$_3$ and SRaaiNR (2 equivalent of ruthenium) in 2-methoxyethanol at N$_2$ atmosphere and precipitation by NaClO$_4$ (*vide* Section 3). The reaction of RuCl$_3$ and SRaaiNR in 1:2 mole proportion in methanol and precipitation of the products by NaClO$_4$ give the compound [Ru(SRaaiNR)(***S***RaaiNR)Cl](ClO$_4$) (**4a/4b**) [SRaaiNR represents tridentate *N,N′*,S-chelator and ***S***RaaiNR as *N,N′*-bidentate chelator where ***S*** does not coordinate]. The molar conductance measurements of the compounds **3** and **4** in MeCN support 1:2 (Λ_M = 150–160 Ω^{-1} mol^{-1} cm^{-1}) and 1:1 (Λ_M = 80–90 Ω^{-1} mol^{-1} cm^{-1}) electrolyte, respectively. Besides, microanalytical data and spectral data support the composition. The structural confirmation in case of **4b** has been carried out by single crystal X-ray diffraction measurement.

RuCl$_3$ and SRaaiNR (1:2 mole ratio) in methanol is absorbed on activated silica gel surface (60–120 mesh) and dried in air. Dry mass is then irradiated (frequency 450 W) with microwave. CH$_2$Cl$_2$ extract is purified by chromatography using MeCN solution of NH$_4$PF$_6$ as eluent. The compound is then characterized by different analytical techniques and structure is confirmed in one case by single crystal X-ray diffraction study. There are two tris-chelated ligands about Ru(II) and one of them shows elimination of R group from S–R motif. Thus the solid surface activated reaction shows C–S cleavage which is denoted **S**aaiNR and the compound is abbreviated as [Ru(SRaaiNR)(**S**aaiNR)](PF$_6$) (**5a/5b**).

2.2. Infrared and ^{1}H NMR spectra

Infrared spectra of the complexes exhibit ν(N=N) and ν(C=N) at 1376–1386 and 1584–1592 cm^{-1}, respectively (see Section 3.3). The azo (–N=N–) stretching is significantly shifted to lower frequency region compared to free ligand value (1400–1410 cm^{-1}) [19] which supports efficient back donation, dπ(Ru(II)) → π^*(azo). The normal mode analysis of DFT computed optimized structure has calculated stretching frequencies. In general the computed frequencies of functional groups appeared at lower frequency region; for example calculated ν(N=N) appears at ~1360 cm^{-1} while observed frequency is ~1380 cm^{-1} and theoretical ν(C=N) is 1560 cm^{-1} and experimental value is ~1585 cm^{-1}. The ν(ClO$_4$) appears at 1090–1094 cm^{-1} and a weak band at 625–630 cm^{-1} for **3** and **4**; ν(PF$_6$) appears at 840–842 cm^{-1} for **5**.

The ^{1}H NMR spectra of the complexes are recorded in CDCl$_3$ (proton numbering pattern is shown in Scheme 1) and protons are assigned on the basis of spin–spin interaction. Data are set out in Supplementary Table S1. The alkylation of imidazole is supported by disappearance of δ(N–H) at ~10.30 ppm (of **1**) and the appearance of alkyl signal at 1.5–4.5 ppm for **2**: The N(1)–Me (**2a**) appears as singlet at *ca.* 4.04 ppm; N–CH$_2$–CH$_3$ (**2b**) shows a quartet for –CH$_2$– at *ca.* 4.46 (9.0 Hz) and a triplet at *ca.* 1.48 (8.0 Hz) ppm. Imidazoles 4-H and 5-H appear as broad singlet at 7.25–7.29 and 7.07–7.14 ppm, respectively. Thiomethyl group (–S–Me) also exhibits a singlet at 2.42 ppm in SMeaaiNMe (**2a**). The SEtaaiNEt (**2b**) shows two quartets [4.46 (9.0 Hz) and 2.99 (8.0 Hz) ppm for –CH$_2$– protons of N–**CH$_2$**–(CH$_3$) and S–**CH$_2$**–(CH$_3$), respectively] and two triplets [at 1.48 (8.0 Hz) and 1.31 (8.0 Hz) ppm for –(N–CH$_2$)**CH$_3$** and –(S–CH$_2$)**CH$_3$**, respectively]. Thiophenyl protons (8-H to 11-H) have been influenced by S–R substituents. The 11-H and 8-H appear as a doublet at *ca.* 7.80–7.86 (8.0 Hz) and 7.18–7.22 (8.0 Hz) ppm, respectively. The closer proximity of electron withdrawing –N=N– group may be the reason for higher δ of 11-H.

In the complexes the aryl protons (8-11 H) suffer downfield shifting by 0.2–0.4 ppm while imidazole 4-H and 5-H are shifted to downfield by 0.4–0.7 ppm relative to free ligand values. The

downfield shift of aromatic protons is in support of electron density shifting away from the ligand which could possible by coordination of the ligands to Ru(II). The R groups in –S–R show very interesting signal modulation. The R groups of coordinated S (**3a/3b**) show 0.2 ppm downfield shifting. The presence of uncoordinated –SR groups in **4a/4b** are also supported by appearance of two signals. Thus ^{1}H NMR signal pattern supports retention of structures in solution-phase also.

2.3. Molecular structure

2.3.1. [Ru(SEtaaiNEt)(*S*EtaaiNEt)Cl](ClO$_4$) (*4b*)

The molecular structure of [Ru(SEtaaiNEt)(*S*EtaaiNEt)Cl](ClO$_4$) (**4b**) is given in Fig. 1. The coordination sphere around Ru is distorted octahedral as revealed from the metric parameters (Table 1). Out of two chelating ligands one acts as tridendate *N*,*N*′,S (imidazole-N (N(7)), azo-N (N(5)), thioether-S (S(1)) and other is *N*,*N*′-bidentate chelator (N(1), N(3)). Sixth coordination position is occupied by Cl. ClO_4^- balances charge of the compound. The N–Ru–N′ chelate angles are ∠N(5)–Ru–N(7), 77.40(11)° and ∠N(1)–Ru–N(2), 75.68(10)° for two different ligands. Remaining chelate angle is ∠N(5)–Ru–S(1), 84.39(8)°. The distortion from octahedral geometry is certainly due to the acute chelate bite angle (∼76°). The planes constituted by tridentate *N*,*N*′,S ligand is deviated significantly from planarity (>0.09 Å) than the chelate plane of bidentate *N*,*N*′-ligand. Each chelate ring is in good plane and no atom deviating by more than 0.07 Å. The stereochemical arrangement is *cis*-N(imidazole) (∠N(3)–Ru–N(7), 97.22(11)°) and *cis*-N(azo) (∠N(1)–Ru–N(5), 99.22(10)°). The coordinated S and Cl are also in *cis*-configuration (∠Cl(1)–Ru–S(1), 92.46(3)°). Atom S2 is disordered over two sites (S2A and S2B).

The Ru–N(imidazole) distances are different for the two coordinated chelating ligands (Ru–N(3), 2.064(3) and Ru–N(7), 2.037(3) Å). The shorter Ru–N distance for tridentate chelating ligand is due to the presence of Ru–S(1) bond *trans* to Ru–N(7) bond, enhancing Ru(dπ) → N(pπ) back donation. Similarly, the Ru–N(azo) distances: Ru–N(5) (1.976(3) Å) is shorter than Ru–N(1) (2.007(2) Å) because of the presence of Cl(1) *trans* to N(1). It is interesting to note that Ru–N(azo) distances are shorter than Ru–N(imidazole) which is mainly due to involvement of π-backbonding of dπ(Ru) electrons to π*(azo) of azoimine ligand [23,24]. The N=N distances are N(1)–N(2), 1.278(3); N(5)–N(6), 1.286(3) Å which are elongated slightly from that of free ligand value [25]. The coordination can lead to decrease in the N–N bond order due to both σ-donor and π-acceptor characters of the ligand – the later character having more pronounced effect. The elongation in the N–N distance is the indication of the existence of considerable π-bonding with major involvement of the azo group. The Ru–Cl(1) distance 2.3865(13) Å appears in the reported range [24].

Table 1
Selected bond distances (Å) and bond angles (°) of [Ru(SEtaaiEt)$_2$Cl]ClO$_4$ (**4b**) and [Ru(SEtaaiEt)(SaaiEt)]PF$_6$·(OH$_2$)$_2$ (**5b**) on X-ray crystallography and singlet ground state geometries.

(**4b**)			(**5b**)		
X-ray data		Theo.	X-ray data		Theo.
Ru–N(1)	2.007(2)	2.011	Ru–N(1)	2.009(6)	2.038
Ru–N(3)	2.064(3)	2.048	Ru–N(4)	1.920(6)	2.978
Ru–N(5)	1.976(3)	2.042	Ru–N(5)	2.079(6)	2.104
Ru–N(7)	2.037(3)	2.074	Ru–N(8)	1.959(5)	2.029
Ru–S(1)	2.3412(10)	2.414	Ru–S(1)	2.3484(19)	2.382
Ru–Cl(1)	2.3731(9)	2.424	Ru–S(2)	2.357(2)	2.465
N(1)–N(2)	1.278(3)	1.325	N(3)–N(4)	1.344(6)	1.333
N(5)–N(6)	1.286(3)	1.320	N(7)–N(8)	1.304(6)	1.328
N(1)–Ru–N(3)	75.68(10)	78.10	N(1)–Ru–N(4)	76.5(2)	77.58
N(5)–Ru–N(7)	77.40(11)	76.39	N(5)–Ru–N(8)	76.5(2)	76.83
S(1)–Ru–N(5)	84.39(8)	91.96	S(1)–Ru–N(4)	83.62(19)	83.48
			S(2)–Ru–N(8)	83.41(17)	83.87

2.3.2. [Ru(SEtaaiNEt)(*S*aaiNEt)](PF$_6$) (*5b*)

The molecular structure is shown in Fig. 2 and selected bond parameters are set out in Table 1. Ru is in distorted octahedral position, which is revealed from the metric parameters. Both the ligands serve as tridentate *N*,*N*′,S-chelator. Significant difference between two ligands is the cleavage of one S–Et group and formation of thiolato (S$^-$) donor centre. PF_6^- balances charge of the compound. The donor groups are associated with *cis*-N(imidazole), *trans*-N(azo) and *cis*-S. The N–Ru–N′ chelate angles are ∠N(1)–Ru–N(4), 76.5(2)° and ∠N(5)–Ru–N(8), 76.50(2)° for two different ligands. Other chelate angles are ∠N(4)–Ru–S(1), 83.62(19)° and ∠N(8)–Ru–S(2), 83.41(17)°.

The Ru–N(imidazole) distances are Ru–N(1), 2.009(6) and Ru–N(5), 2.079(6) Å and Ru–N(azo) distances are Ru–N(4),

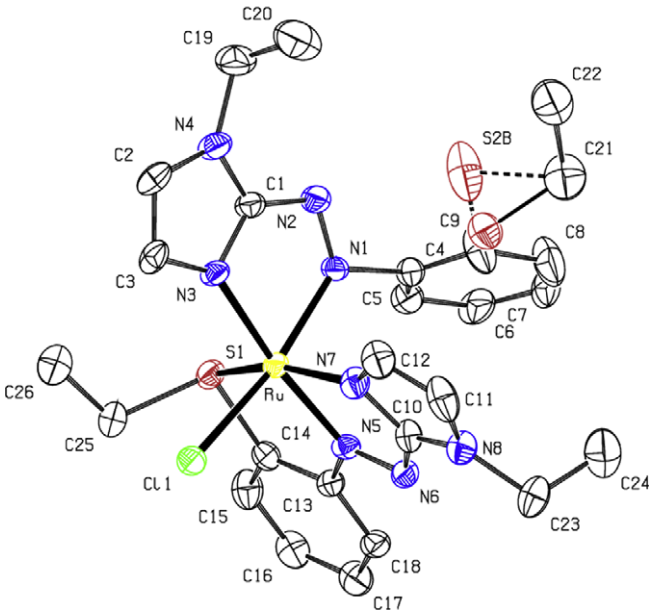

Fig. 1. ORTEP plot of **4b**$^+$, H atoms have been omitted.

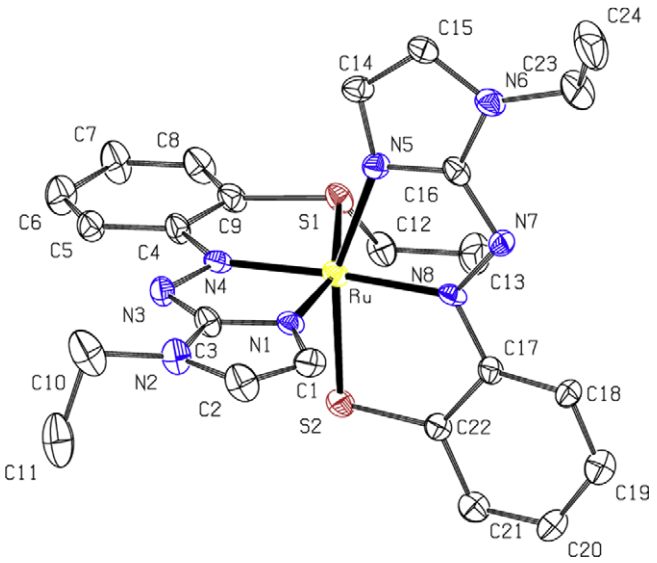

Fig. 2. ORTEP plot of **5b**$^+$, H atoms have been omitted.

1.920(6) and Ru–N(8), 1.959(5) Å). The Ru–N distances in Ru(SEtaaiNEt) chelate is longer than Ru(**S**aaiNEt) chelate system. The Ru–N(azo) distances are smaller than Ru–N(imidazole) distances. The N=N distances are N(3)–N(4), 1.344(6); N(7)–N(8), 1.304(6) Å those are longer than azo distance of **4b**. The presence of thiolato Ru–S bond may be the reason for better π–back bonding. Thioether coordination (Ru–S(1), 2.3484(19) Å) does not differ significantly to Ru–S(thiolato) (Ru–S(2), 2.357(2) Å) distance.

2.4. DFT calculation

The molecular structures of **3b**, **4b** and **5b** are optimized by using B3LYP/DFT calculations of G03 programme. The computed structures well reproduce the experimental structures for **4b** and **5b** (Table S2). Theoretical Ru–N bond lengths are about 0.01–0.07 Å longer than that of observed one. The experimental Ru–Cl distances are shorter by 0.051 Å than theoretical data for **4b**. The Ru–S distances are also elongated in calculated structures by 0.03–0.07 Å.

The orbital energies along with contributions from the ligands and metal are given in Supplementary Table S3 and Fig. 3 depicts the features of some selected occupied and unoccupied frontier orbitals. Energy level correlations along with contribution of molecular orbitals are given in Fig. 4. The electronic structures of the complexes are characterized by high degree of mixing between Ru(dπ) and ligand-π/pπ orbitals. The three low energy occupied molecular orbitals (HOMO to HOMO-2) of **3b** have 24–27% Ru and 73–76% ligand character. The HOMO−3 is mainly contributed by ligand while HOMO−4 and HOMO−6 have 32–43% Ru along with 57–68% ligand character. The orbitals, HOMO−7 to HOMO−10 are mostly contributed by ligand group of orbitals. The LUMO has 90% ligand character and mainly concentrated on azo-π^* orbitals (48%) and an energy gap with HOMO of 2.40 eV in gas phase calculation. The next higher energy unoccupied molecular orbitals (HOMO−1, HOMO−3 to HOMO−5) also have 79–91% ligand contribution whereas in HOMO−2 has an increased amount of Ru character (42%).

In **4b** the HOMO, HOMO−1 and HOMO−3 have 29–43% Ru and 50–53% ligand along with small contribution from Cl. The HOMO−2 and HOMO−4 to HOMO−10 are constructed by the azo-ligand (70–95%). The LUMO has 87% ligand (N=N, 53) character and the HOMO−LUMO energy gap is 2.54 eV. The other low energy LUMOs (LUMO+1 to LUMO+5) predominantly have ligand(π^*) character. The HOMOs and LUMOs for **5b** follow the similar character as **3b** and **4b** with HOMO−LUMO gap of 1.96 eV. The results in acetonitrile phase are more or less following same sequence of gas phase calculation. The results of calculation are comparable with reported data [26].

2.5. TDDFT calculations and spectral analysis

The electronic absorption spectra are measured at room temperature in acetonitrile, and the experimental absorption bands are assigned using the singlet-excited states calculated with TDDFT/CPCM method. Absorption spectra of the complexes in acetonitrile are shown in Fig. 5 and data are collected in Table 2. Some of the calculated excitation wavelength and their assignment are given in Table 3 and full detail is given in *Table* S4 in Supplementary material. As seen, TDDFT calculations well reproduce the absorption spectrum of the complexes measured in acetonitrile.

A high intense transition band, at <400 nm originates predominately in the HOMO−4/HOMO−5 → LUMO/LUMO+1 transition, and mainly intra or inter-ligand charge transfer transitions ($n \rightarrow \pi^*$ and $\pi \rightarrow \pi^*$). Visible region spectra of the complexes also exhibit broad intense transitions at 450–470 nm and 510–560 nm. These bands arise due to HOMO−2/HOMO−1 → LUMO/LUMO+1 transitions. In addition to these intense bands the complexes **3b** and **5b** show low energy weak transition at 730–740 and 925–935 nm, respectively. The TDDFT/CPCM result predicts that it originates in the HOMO → LUMO/LUMO+1 transition. Since, HOMO, HOMO−1 and HOMO−2 are metal and ligand characteristics, and the LUMO/LUMO+1 completely concentrated on ligand; the low energy transitions can be assign as mixed MLCT and ILCT

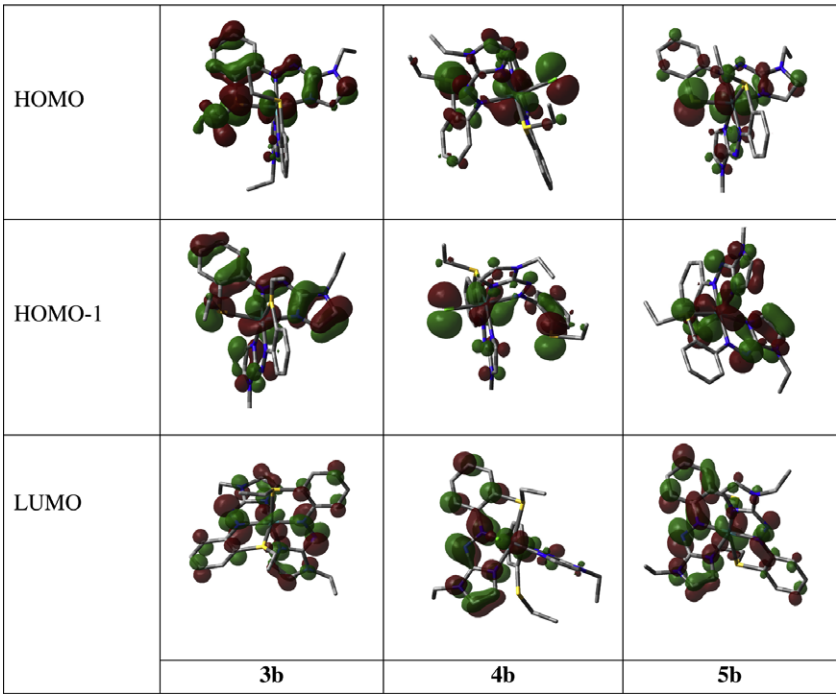

Fig. 3. HOMO, HOMO−1 and LUMO of **3b**, **4b** and **5b** in gas phase (isosurface cutoff value = 0.03).

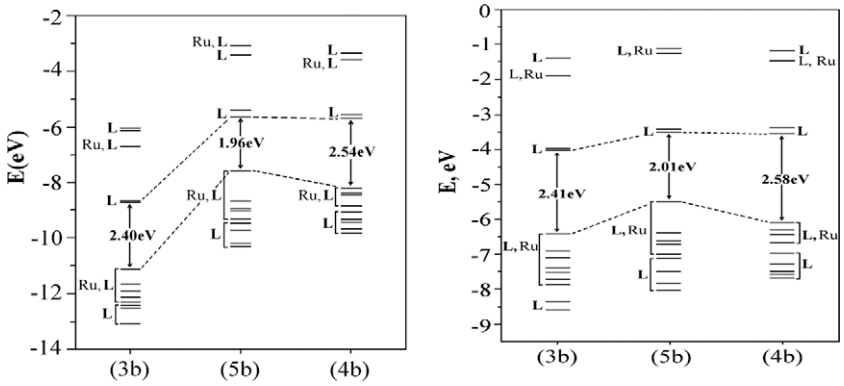

Fig. 4. Energy level co-relation diagram in gas phase (left) and in acetonitrile (right).

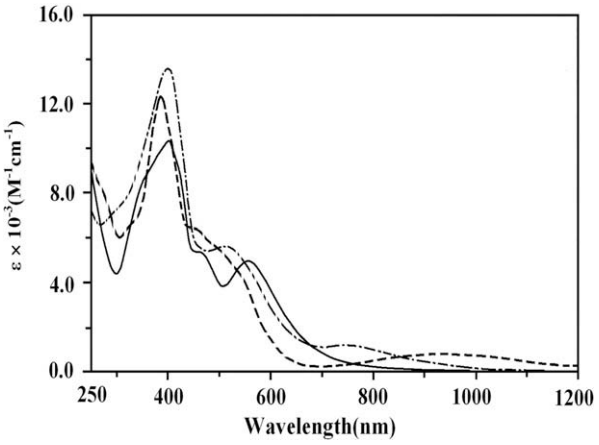

Fig. 5. Absorption spectra of (**3b**)(-.-.-), (**4b**) (—) and (**5b**) (———) in acetonitrile.

origin or a delocalized MLLCT (metal–ligand to ligand charge transfer) description can be used.

The intensity of these transitions has been assessed from oscillator strength (*f*). In both gas and acetonitrile phases the longest wavelength band appears in NIR region, >700 nm. This transition is weak as evident from very low *f* value. Transition of high *f* is observed at 380–420 nm ($f > 0.1$) and have been assigned π–π^* transition.

2.6. Electrochemistry

The redox data of the complexes are summarised in Table 2. The complexes show Ru(III)/Ru(II) couple (Fig. 6) when scanned in the potential range 0.0–2.0 V. The response is quasi reversible in nature as it is evident from their peak-to-peak separation ($\Delta E_p > 100$ mV). The nature of voltammogram does not change with scan rate (50–250 mV s^{-1}). One electron stoichiometry of the couple has been confirmed by the current height measurement by DPV and on comparing with couple of $[Fe(CN)_6^{4-}]/[Fe(CN)_6^{3-}]$.

The DFT calculations show that HOMO of the complexes has Ru contribution and ligand contributes to constitute LUMO (major participation from azo group) (*Table* S3, Supplementary material). Thus the oxidation may be assigned to the involvement of metal orbitals and the reduction is azo function of the ligands. Ru(III)/Ru(II) redox couples in **5a**–**5b** are found lowest than that of **3a**–**3b** and **4a**–**4b** which reflect higher electron influx on metal centre in **5a/5b** compare to **3a/3b** and **4a/4b** (Fig. 6). The calculated Mulliken charge on Ru is considerably lower than the formal charge +2 and is found 0.540, 0.439 and 0.366 in complex **3b**, **4b** and **5b**, respectively (*Supplementary* Table S5). Data in *Supplementary* Table S3 show that the stability order of HOMOs of the complexes is **3b**(−11.13 eV) > **4b**(−8.28 eV) > **5b**(−7.61 eV) and so the metal oxidation follows the reverse order. Thiolato-S is certainly better σ-donor than thioether-S and could be responsible for lowest potential in the complexes **5**. Azo reductions are also equally affected by number of Ru–S bonds, thioether-S or thiolato-S i.e., E(azo/azo$^-$) and E(azo$^-$/azo$^{=}$) data are anodically shifted as **5** → **4** → **3**.

2.7. Conclusion

1-Alkyl-2-{(*o*-thioalkyl)phenylazo}imidazoles are used to synthesise ruthenium(II) complexes. Reaction phase and solvents influence the chemical characteristic of the products. In high boiling solvent, 2-methoxyethanol, the reaction separates the product where ligand behaves as tridentate *N*,*N*′,S-chelator while in methanol (relatively low boiling solvent) one of the two chelating ligands acts as bidentate *N*,*N*′-chelator. The reaction in silica surface at solid state upon microwave irradiation has isolated a product that shows C–S cleavage. The complexes show intense MLCT transition along with ILCT and affect the metal redox property. The DFT and TDDFT computation have been carried out to

Table 2
UV–Vis spectra[a] and cyclic voltammetric[b] data

Complex	λ_{max} (nm)[a] ($10^{-3} \in M^{-1}$ cm^{-1})	Cyclic voltammetric data[b]	
		$E_{Ru(III)/Ru(II)}$, V (ΔE_p, mV)	Ligand reduction, V (ΔE_p, mV)
(**3a**)	730(1.82), 510(6.28), 400(14.54)	1.48 (110)	−0.52(80), −0.84(90), −1.42(130)
(**3b**)	740(1.88), 515(5.87), 395(14.22)	1.49 (110)	−0.48(80), −0.88(90), −1.44(140)
(**4a**)	558 (5.50), 466 (5.97), 399(11.87)	1.30(110)	−0.44(70), −0.80(95), −1.36(150)
(**4b**)	556 (5.05), 468 (5.24), 399 (10.06)	1.32(110)	−0.45(80), −0.81(90), −1.38(145)
(**5a**)	922 (1.34), 546 (5.04), 456 (7.97), 390 (13.74)	1.21 (110)	−0.78(80), −0.86(90), −1.38(140)
(**5b**)	932 (1.26), 550 (4.75), 462 (6.25), 388 (12.12)	1.22 (110)	−0.79(70), −0.97(90), −1.40(160)

[a] In MeCN.
[b] Solvent: MeCN, Pt-disk working electrode, SCE reference and Pt–wire auxiliary electrode, [*n*-Bu_4N](ClO_4) supporting electrolyte, scan rate 50 mV s^{-1}, $E = 0.5\ (E_{pa} + E_{pc})$ V, $\Delta E_p = (E_{pa} - E_{pc})$, mV, E_{pa} = anodic peak potential, E_{pc} = cathodic peak potential.

Table 3
Selected list of calculated (TDDFT) excitation energies for [Ru(SEtaaiEt)$_2$] $(ClO_4)_2$(**3b**), [Ru(SEtaaiEt)(***S***EtaaiEt)Cl]ClO_4(**4b**) and [Ru(SEtaaiEt)(**S**aaiEt)]PF_6 (**5b**) in acetonitrile

Excited state	E (eV)	λ, nm($f \times 10^3$)	Major contribution	Character[a]
3b				
1	1.61	770.6(18.4)	(82%)HOMO → LUMO	MLCT, ILCT
2	1.65	750.8(20.0)	(81%)HOMO → L+1	MLCT, ILCT
5	2.48	499.4(122.1)	(32%)H−2 → L+1, (26%)H−1 → LUMO	ILCT
12	2.99	413.4(321.9)	(33%)H−3 → L+1, (21%)H−3 → LUMO	ILCT
14	3.12	397.4(492.3)	(37%)H−5 → L+1, (18%)H−5 → LUMO	MLCT, ILCT
4b				
3	2.02	612.4(9.4)	(35%)H−2 → L+1, (24%)H−1 → L+1	MLCT, ILCT
6	2.15	575.6(8.5)	(39%)H−3 → LUMO, (21%)H−2 → L+1	MLCT, ILCT
7	2.39	518.5(129.2)	(52%)H−2 → LUMO	MLCT, ILCT
8	2.71	457.6(107.8)	(51%)H−3 → L+1	MLCT, ILCT
10	2.98	415.1(200.6)	(62%)H−4 → LUMO	ILCT
11	3.04	406.9(151.3)	(36%)H−4 → L+1	ILCT
5b				
2	1.32	937.4(23.2)	(84%)HOMO → L+1	MLCT, ILCT
4	2.18	569.0(16.5)	(37%)H−2 → LUMO, (35%)H−1 → L+1	MLCT, ILCT
5	2.28	543.8(23.3)	(35%)H−3 → LUMO, (18%)H−1 → LUMO	MLCT, ILCT
7	2.61	473.8(213.6)	(35%)H−2 → L+1, (26%)H−3 → LUMO	MLCT, ILCT
12	3.08	401.7(225.0)	(64%)H−4 → L+1	ILCT
13	3.16	392.3(555.2)	(48%)H−5 → LUMO	ILCT

[a] ILCT = intra/inter-ligand charge transfer; MLCT = metal to ligand charge transfer.

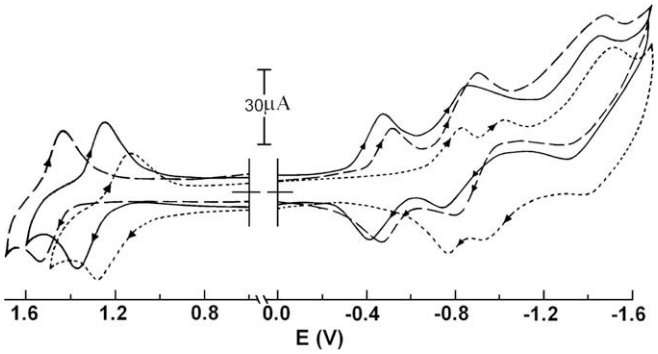

Fig. 6. Cyclic voltammogram of **3b** (- - - -), **4b** (—) and **5b** (· · · · ·) in acetonitrile.

explain the electronic structure and vibrational, electronic spectra and redox properties of the complexes.

3. Experimental

3.1. Materials

$RuCl_3{\cdot}3H_2O$ was purchased from Arrora Matthey, Kolkata, India. Imidazole and all other organic chemicals and inorganic salts were available from Sisco Research Lab, Mumbai, India. The purification of acetonitrile and preparation of *n*-tetra butylammonium perchlorate [*n*-Bu_4N][ClO_4] for electrochemical work were done as before [13]. Dinitrogen was purified by bubbling through an alkaline pyrogallol solution. Solvents were distilled over appropriate drying agents under appropriate condition as per literature under N_2 environment [27]. All other chemicals and solvents were of reagent grade and were used without further purification. Commercially available SRL silica gel (60–120 mesh) was used for column chromatography. The syntheses of the ligands were carried out following the common procedure [19].

3.2. Physical measurements

Microanalytical data (C, H, N) were collected on Perkin–Elmer 2400 CHNS/O elemental analyzer. Spectroscopic data were obtained using the following instruments: UV–Vis spectra, Perkin–Elmer; model Lambda 25. IR spectra (KBr disk, 4000–450 cm^{-1}), Perkin–Elmer; model RX-1; ^1H NMR spectra, Bruker (AC) 300 MHz FTNMR spectrometer. Electrochemical measurements were performed using computer-controlled PAR model 250 VersaStat electrochemical instruments with Pt-disk electrodes. All measurements were carried out under nitrogen environment at 298 K with reference to SCE in acetonitrile using [*n*-Bu_4N][ClO_4] as supporting electrolyte. The reported potentials are uncorrected for junction potential.

3.3. Synthesis of complexes

3.3.1. Synthesis of [Ru(SMeaaiNMe)$_2$](ClO$_4$)$_2$ (*3a*) and [Ru(SMeaaiNMe)$_2$(Cl)] (ClO$_4$) (*4a*)

$RuCl_3{\cdot}3H_2O$ (0.27 g, 1.02 mmol) was dissolved in 20 ml 2-methoxyethanol and refluxed for an hour under N_2 atmosphere. To the resulting green solution 10 ml 2-methoxyethanolic solution of 1-methyl-2-[*o*-(thiomethyl)phenylazo]imidazole (SMeaaiNMe) (0.5 g, 2.15 mmol) was added and reflux for another 4 h. The solvent was completely removed using rotaevaporator. Brown gummy mass so left was dissolved in minimum volume of methanol and aqueous solution of $NaClO_4$ was added to precipitate the product. The precipitate was filtered and washed with cold water, and finally dried in *vacuo* over P_4O_{10}. The dry mass was then dissolved in minimum volume of CH_2Cl_2 and subjected to chromatography on a silica gel column (60–120 mesh). A red band was eluted with C_6H_6–CH_3CN (5:1, v/v). This was collected and evaporated slowly in air. The yield was 65%.

Anal. Calc. for $C_{22}H_{24}N_8O_8S_2Cl_2Ru$ (**3a**): C, 35.29; H, 3.21; N, 14.97. Found: C, 35.14; H, 3.18; N, 14.92%. IR_{exp} (KBr, cm^{-1}): ν(C═N) = 1586, ν(N═N) = 1380, $\nu(ClO_4^-)$ = 1090, 626. ^1H NMR ($CDCl_3$): δ 8.44 (H_{11}, d, J = 7.5), 7.94 (H_4, s), 7.74 ($H_{9,10}$, m), 7.56 (H_8, d, J = 7.0), 7.44 (H_5, s), 4.38 (N–CH_3, s), 2.60 (S–CH_3, s). Anal. Calc. for $C_{26}H_{32}N_8O_8S_2Cl_2Ru$ (**3b**): C, 38.81; H, 3.98; N, 13.93. Found: C, 38.76; H, 3.97; N, 13.90%. IR_{exp} (KBr, cm^{-1}): ν(C═N) = 1584, ν(N═N) = 1382, $\nu(ClO_4^-)$ = 1092, 627. IR_{theo} (cm^{-1}): ν(C═N) = 1560, 1565, ν(N═N) = 1361. ^1H NMR ($CDCl_3$): δ 8.26 (H_{11}, d, J = 7.5), 7.89 (H_4, s), 7.64 ($H_{9,10}$, m), 7.47 (H_8, d, J = 7.0), 7.36 (H_5, s), 4.74 (N–**CH_2**–CH_3, q, J = 8.0), 1.74 (N–CH_2–**CH_3**, t, J = 7.5), 2.96 (S–**CH_2**–CH_3, q, J = 7.5), 1.22 (S–CH_2–**CH_3**, t, J = 7.0).

The synthesis procedure of **4** is similar as mentioned above for **3** but the reaction was carried out in dry methanol. The yield was 60–70%.

Anal. Calc. for $C_{22}H_{24}N_8O_4S_2Cl_2Ru$ (**4a**): C, 38.15; H, 3.47; N, 16.18. Found: C, 38.26; H, 3.49; N, 16.24%. IR_{exp} (KBr, cm^{-1}): ν(C=N) = 1585, ν(N=N) = 1378, ν(Ru–Cl) = 342, $\nu(ClO_4^-)$ = 1091, 625. ^1H NMR ($CDCl_3$): δ 8.62 (H_{11}, d, J = 8.0), 7.88 (H_4, s), 7.78 ($H_{9,10}$, m), 7.61 (H_8, d, J = 7.5), 7.30 (H_5, s), 4.30 (N–CH_3, s), 2.57, 2.53 (S–CH_3, s). Anal. Calc. for $C_{26}H_{32}N_8O_4S_2Cl_2Ru$ (**4b**): C, 41.71; H, 4.28; N, 14.97. Found: C, 41.60; H, 4.25; N, 14.92%. IR_{exp} (KBr, cm^{-1}): ν(C=N) = 1590, ν(N=N) = 1386, ν(Ru–Cl) = 340, $\nu(ClO_4^-)$ = 1094, 630. IR_{theo} (cm^{-1}): ν(C=N) = 1557, 1562, ν(N=N) = 1359, ν(Ru–Cl) = 332. ^1H NMR ($CDCl_3$): δ 8.32 (H_{11}, d, J = 8.0), 7.82 (H_4, s), 7.65 ($H_{9,10}$, m), 7.56 (H_8, d, J = 7.5), 7.26 (H_5, s), 4.58 (N–**CH_2**–CH_3, q, J = 8.0), 1.60 (N–CH_2–**CH_3**, t, J = 7.5), 3.39, 3.36 (S–**CH_2**–CH_3, q, J = 8.0), 1.29, 1.26 (S–CH_2–**CH_3**, t, J = 7.0).

3.3.2. Synthesis of [Ru(SMeaaiNMe)(SaaiNMe)](PF_6) (**5a**)

$RuCl_3 \cdot 3H_2O$ (0.25 g, 0.95 mmol) was dissolved in super dry MeOH (20 ml) and refluxed under dry N_2 gas. The solution color turned to deep green (suggesting reduction of Ru(III) to Ru(II)). The ligand, SMeaaiNMe (0.48 g, 2.07 mmol) was added into the solution and then activated silica gel (60–120 mesh) (15 g) was added in portion wise with stirring continuously to make a paste. The whole mass was then transferred into a silica crucible and dried by passing N_2 gas. Crucible was then placed in the microwave oven and irradiated at 450 W for 5 min × 5 with 10 min interval at each step. Solid surface was then turned into black. It was then cooled and extracted with CH_2Cl_2. Brown–red solution was then chromatographed over alumina column prepared in benzene. Light yellow portion was eluted first by benzene. A dark band was then eluted by MeCN solution of NH_4PF_6 (0.05 g per 50 ml). The eluent was evaporated slowly in air. The crystals were separated. The crystals were isolated by filtration and washed with cold water. It was then dried over $CaCl_2$. Yield: 0.48 g, 72%.

Anal. Calc. for For $C_{21}H_{21}N_8F_6PS_2Ru$ (**5a**): C, 36.26; H, 3.02; N, 16.11. Found: C, 36.08; H, 3.01; N, 16.08%. IR_{exp} (KBr, cm^{-1}): ν(C=N) = 1592, ν(N=N) = 1378, $\nu(PF_6^-)$ = 840. ^1H NMR ($CDCl_3$): δ 8.51 (H_{11}, d, J = 8.0), 7.68 (H_4, s), 7.58 ($H_{9,10}$, m), 7.48 (H_8, d, J = 7.0), 7.40 (H_5, s), 4.33 (N–CH_3, s), 2.56 (S–CH_3, s). Anal. Calc. for $C_{24}H_{27}N_8F_6PS_2Ru$ (**5b**): C, 39.08; H, 3.66; N, 15.20. Found: C, 38.95; H, 3.65; N, 15.16%. IR_{exp} (KBr, cm^{-1}): ν(C=N) = 1590; ν(N=N) = 1376; $\nu(PF_6^-$ = 842. IR_{theo} (cm^{-1}): ν(C=N) = 1557, 1562; ν(N=N) = 1352. ^1H NMR ($CDCl_3$): δ 8.28 (H_{11}, d, J = 7.5), 7.60 (H_4, s), 7.62 ($H_{9,10}$, m), 7.51 (H_8, d, J = 7.0), 7.38 (H_5, s), 4.71 (N–**CH_2**–CH_3, q, J = 7.5), 1.72 (N–CH_2–**CH_3**, t, J = 7.5), 3.00 (S–**CH_2**–CH_3, q, J = 7.5), 1.20 (S–CH_2–**CH_3**, t, J = 7.0).

3.4. X-ray crystal structure analysis

The X-ray quality crystals were grown by slow diffusion of dichloromethane solution into hexane. Details of crystal analyses, data collection and structure refinement data are given in *Supplementary* Table S6. Crystal mounting was done on glass fibers with epoxy cement. Single crystal data collection were performed with Siemens SMART CCD diffractometer using fine focus sealed graphite-monochromatized Mo Kα radiation (λ = 0.71073 Å) for [Ru(SEtaaiNEt)(***S***EtaaiNEt)Cl](ClO_4) (**4b**) (0.28 × 0.20 × 0.18 mm) at 293(2) K and for [Ru(SEtaaiNEt)(SaaiNEt)](PF_6) (**5b**) (0.15 × 0.15 × 0.10 mm) at 295(2) K. Unit cell parameters were determined from least-squares refinement of setting angles with θ in the range $1.60 \leqslant \theta \leqslant 28.36°$ (**4b**), $1.64 \leqslant \theta \leqslant 28.29°$ (**5b**). Of 20 147 collected data 7772 for **4b**, 7474 collected data 2286 for **5b** with $I > 2\sigma(I)$ were used for structure solution. The *hkl* range are $-18 \leqslant h \leqslant 14$, $-13 \leqslant k \leqslant 17$, $-25 \leqslant l \leqslant 23$ for **4b**, $-12 \leqslant h \leqslant 14$, $-15 \leqslant k \leqslant 15$, $-25 \leqslant l \leqslant 32$ for **5b**. Reflection data were recorded using the ω-scan technique. Data were corrected for Lorentz polarization effects and for linear decay. Semi-empirical absorption corrections based on ψ-scans were applied. The structure was solved by direct method for all these compounds using SHELXS-97 and successive difference Fourier syntheses. All non-hydrogen atoms were refined anisotropically. The hydrogen atoms were fixed geometrically and refined using the riding model. All calculations were carried out using SHELXL-97 [28], ORTEP-32 [29] and PLATON-99 [30] programs.

3.5. Computational methods

All computations were performed using the GAUSSIAN03 (G03) [31] software package running under Windows. The Becke's three-parameter hybrid exchange functional and the Lee–Yang–Parr nonlocal correlation functional (B3LYP) [32] was used throughout. Elements except ruthenium were assigned a 6-31G* basis set in our calculations. For ruthenium the Los Alamos effective core potential plus double zeta (LanL2DZ) [33] basis set was employed. Gas and solution-phase optimization was carried out from the geometry obtained from the crystal structure without any symmetry constraints. In all cases, vibrational frequencies were calculated to ensure that optimized geometries represented local minima. The excitation energies were calculated by the TDDFT approach. To check the effect of solvation on the calculated optical absorption spectra, we performed TDDFT calculations of the low lying excitation at the singlet optimized geometry, including solvation effect by means of the nonequilibrium implementation of the polarizable continuum model [34]; as in the experimental conditions, the chosen solvent is acetonitrile. GaussSum [35] was used to calculate the fractional contributions of various groups to each molecular orbital. This is done using Mulliken population analysis.

Acknowledgments

Financial support from the Department of Science and Technology and University Grants Commission-CAS programme, New Delhi are gratefully acknowledged.

Appendix A. Supplementary material

CCDC 601286 and 673712 contain the supplementary crystallographic data the structures [Ru(SEtaaiNEt)(***S***EtaaiNEt)Cl](ClO_4) (**4b**) and [Ru(SEtaaiNEt)(**S**aaiNEt)](PF_6) (**5b**), respectively. These data can be obtained free of charge from The Cambridge Crystallographic Data Centre via www.ccdc.cam.ac.uk/data_request/cif. Supplementary data associated with this article can be found, in the online version, at doi:10.1016/j.jorganchem.2009.06.021.

References

[1] W.Y. Wong, S.H. Cheung, S.M. Lee, S.Y. Leung, J. Org. Chem. 596 (2000) 36.
[2] L. Carlucci, G. Ciaxi, D.M. Proserpio, S. Rizzato, New J. Chem. 27 (2003) 483.
[3] T. Akasaka, T. Mutai, J. Otsuki, K. Araki, J. Chem. Soc., Dalton Trans. (2003) 1537.
[4] F. Casalbani, Q.G. Mulazzani, C.D. Clark, M.Z. Hoffman, P.L. Orizondo, M.W. Perkovic, D.P. Rillema, Inorg. Chem. 93 (1998) 205.
[5] V.W.-W. Yan, V.C.-Y. Lan, K.-K. Cheung, J. Chem. Soc., Chem. Commun. (1995) 259.
[6] S. Frantz, J. Fiedler, I. Hartenbach, T. Schleid, W. Kaim, J. Organomet. Chem. 689 (2004) 3031.
[7] B.K. Ghosh, A. Chakravorty, Coord. Chem. Rev. 95 (1989) 239.
[8] B.K. Santra, G.A. Thakur, P. Ghosh, A. Pramanik, G.K. Lahiri, Inorg. Chem. 35 (1996) 3050.
[9] A.C. Cope, R.W. Siekman, J. Am. Chem. Soc. 87 (1965) 3272.
[10] S. Ganguly, S. Chattopadhyay, C. Sinha, A. Chakravorty, Inorg. Chem. 39 (2000) 2954. and references therein.
[11] R. Aharyya, F. Basuli, R.Z. Wang, T.C. Mak, S. Bhattacharya, Inorg. Chem. 43 (2004) 704. and references therein.

[12] A.H. Velders, K. van der Schilden, A.C.G. Hotze, J. Reedijk, H. Kooijman, A.L. Spek, J. Chem. Soc., Dalton Trans. (2004) 448.
[13] P. Byabartta, J. Dinda, P.K. Santra, C. Sinha, K. Panneerselvam, F.L. Liao, T.H. Lu, J. Chem. Soc., Dalton Trans. (2001) 2825.
[14] S. Senapati, U.S. Ray, P.K. Santra, C. Sinha, J.D. Woolins, A.M.Z. Slawin, Polyhedron 21 (2002) 753.
[15] N. Maiti, S. Pal, S. Chattopadhyay, Inorg. Chem. 40 (2001) 2204. and references therein.
[16] S. Senapati, Sk. Jasimuddin, C. Sinha, Indian J. Chem., Sect. A 45A (2006) 1153.
[17] (a) G. Wilkinson, F.G.A. Stone, E.W. Abel (Eds.), Comprehensive Organometallic Chemistry, Pergamon Press, New York, 1982;
(b) J. Reedijk, in: G. Wilkinson, J.A. McCleverty (Eds.), Comprehensive Coordination Chemistry, vol. 2, Pergamon, Oxford, UK, 1987;
(c) F.A. Cotton, G. Wilkinson, Advanced Inorganic Chemistry, 5th ed., Wiley-Intersciences, New York, 1994.
[18] (a) K. Kalyansundaram, Coord. Chem. Rev. 46 (1982) 159;
(b) S. Serroni, S. Campagna, F. Puntoriero, C.D. Pietro, N.D. McClenaghan, F. Loisean, Chem. Soc. Rev. 30 (2001) 367;
(c) L.A. Garcia-Escudero, D. Miguel, J.A. Turiel, J. Organomet. Chem. 691 (2006) 3434.
[19] D. Banerjee, U.S. Ray, Sk. Jasimuddin, J.-C. Liou, T.-H. Lu, C. Sinha, Polyhedron 25 (2006) 1299.
[20] (a) T. Schaub, M. Backes, U. Radius, Chem. Commun. (1996) 1359;
(b) T.-Y. Luh, Z.-J. Ni, Synthesis (1990) 89;
(c) C.T. Ng, X. Wang, T.Y. Luh, J. Org. Chem. 53 (1988) 2536.
[21] (a) K. Pramanik, U. Das, B. Adhikari, D. Chopra, H. Stoeckli-Evans, Inorg. Chem. 47 (2008) 429;
(b) C. Huang, S. Gou, H. Zhu, W. Huang, Inorg. Chem. 46 (2007) 5537.
[22] (a) D. Shimizu, N. Takeda, N. Tokitoh, Chem. Commun. (2006) 177;
(b) E. López-Torres, M.A. Mendiola, C.J. Pastor, Inorg. Chem. 45 (2006) 3103.
[23] (a) T.K. Misra, D. Das, C. Sinha, P.K. Ghosh, C.K. Pal, Inorg. Chem. 37 (1998) 1672;
(b) P.K. Santra, T.K. Misra, D. Das, C. Sinha, A.M.Z. Slawin, J.D. Woollins, Polyhedron 18 (1999) 2869;
(c) P. Byabartta, P.K. Santra, T.K. Misra, C. Sinha, C.H.L. Kennard, Polyhedron 20 (2001) 905;
(d) Sk. Jasimuddin, P. Byabartta, G. Mostafa, T.-H. Lu, C. Sinha, Polyhedron 23 (2004) 727.
[24] (a) S. Goswami, A.R. Chakravarty, A. Chakravorty, Inorg. Chem. 20 (1981) 2246. 22 (1983) 602;
(b) G.K. Lahiri, S. Bhattacharya, S. Goswami, A. Chakravorty, J. Chem. Soc., Dalton Trans. (1990) 561;
(c) N. Bag, A. Pramanik, G.K. Lahiri, A. Chakravorty, Inorg. Chem. 31 (1992) 40;
(d) R. Samanta, P. Munshi, B.K. Santra, N.K. Loknath, M.A. Sridhar, J.S. Prasad, G.K. Lahiri, J. Organomet. Chem. 579 (1999) 311.
[25] J. Otsuki, K. Suwa, K. Narutaki, C. Sinha, I. Yoshikawa, K. Araki, J. Phys. Chem. A 109 (2005) 8064.
[26] A. Gabrielsson, S. Zalis, P. Matousek, M. Towrie Jr., A. Vleck, Inorg. Chem. 43 (2004) 7380.
[27] A.I. Vogel, Vogel's Textbook of Practical Organic Chemistry, 5th ed., Prentice Hall, 1989.
[28] (a) G.M. Sheldrick, SHELXS-97, Program for the Solution of Crystal Structure, University of Gottingen, Germany, 1997;
(b) G.M. Sheldrick, SHELXL 97, Program for the Refinement of Crystal Structure, University of Gottingen, Germany, 1997.
[29] L.J. Farrugia, J. Appl. Cryst. 30 (1997) 565.
[30] A.L. Spek, PLATON, Molecular Geometry Program, University of Utrecht, The Netherlands, 1999.
[31] M.J. Frisch, G.W. Trucks, H.B. Schlegel, G.E. Scuseria, M.A. Robb, J.R. Cheeseman, J.A. Montgomery Jr., T. Vreven, K.N. Kudin, J.C. Burant, J.M. Millam, S.S. Iyengar, J. Tomasi, V. Barone, B. Mennucci, M. Cossi, G. Scalmani, N. Rega, G.A. Petersson, H. Nakatsuji, M. Hada, M. Ehara, K. Toyota, R. Fukuda, J. Hasegawa, M. Ishida, T. Nakajima, Y. Honda, O. Kitao, H. Nakai, M. Klene, X. Li, J.E. Knox, H.P. Hratchian, J.B. Cross, V. Bakken, C. Adamo, J. Jaramillo, R. Gomperts, R.E. Stratmann, O. Yazyev, A.J. Austin, R. Cammi, C. Pomelli, J.W. Ochterski, P.Y. Ayala, K. Morokuma, G.A. Voth, P. Salvador, J.J. Dannenberg, V.G. Zakrzewski, S. Dapprich, A.D. Daniels, M.C. Strain, O. Farkas, D.K. Malick, A.D. Rabuck, K. Raghavachari, J.B. Foresman, J.V. Ortiz, Q. Cui, A.G. Baboul, S. Clifford, J. Cioslowski, B.B. Stefanov, G. Liu, A. Liashenko, P. Piskorz, I. Komaromi, R.L. Martin, D.J. Fox, T. Keith, M.A. Al-Laham, C.Y. Peng, A. Nanayakkara, M. Challacombe, P.M.W. Gill, B. Johnson, W. Chen, M.W. Wong, C. Gonzalez, J.A. Pople, Gaussian Inc., Wallingford CT, 2004.
[32] C. Lee, W. Yang, R.G. Parr, Phys. Rev. B 37 (1988) 785.
[33] P.J. Hay, W.R. Wadt, J. Chem. Phys. 82 (1985) 270.
[34] M. Cossi, V.J. Barone, J. Chem. Phys. 115 (2001) 4708.
[35] N.M. O'Boyle, A.L. Tenderholt, K.M. Langner, J. Comput. Chem. 29 (2008) 839.